IEEE Access
Multidisciplinary | Rapid Review | Open Access Journal

Received 19 January 2024, accepted 29 January 2024, date of publication 22 February 2024, date of current version 5 March 2024.

Digital Object Identifier 10.1109/ACCESS.2024.3368889

RESEARCH ARTICLE

Wireless Power Supply Sensing Tags Based on Anti-Collision Algorithm for Sensing Systems

DANENG PI
School of Electrical Engineering and Automation, Hubei Normal University, Huangshi 435002, China
e-mail: pilaoshi1966@163.com

ABSTRACT In wireless sensor networks, sensing tags are battery powered, which also limits the battery life. Therefore, it is particularly important to study self powered sensing tags. At present, passive wireless identification systems can achieve self powered communication through tags. However, wireless power supply sensing systems have problems such as low efficiency and short communication distance. To reduce the power consumption of sensing tags and improve the efficiency of sensing systems, a passive wireless low-power hydrogen concentration sensing system is designed. To further reduce the power consumption of sensing tags, a passive wireless magnetic field intensity sensing system is developed. In addition, to solve the low efficiency of multiple sensing labels in wireless power supply sensing systems, an efficient anti-collision algorithm based on dynamic binary query trees is designed. According to the research results, in the cold start indoor environment, the energy collection rate of the sensing tag designed in the research was 0.081mJ/s, and the energy collection efficiency was 25.7%. In single/dual sensor mode, the maximum values of sensing error were 2.1% and 5.2%, respectively. The maximum recognition time of the anti-collision algorithm based on dynamic multi base query tree was 2.78s, and the minimum value was 1.31s. The research results can provide methodological and technical support for the improvement of wireless power supply sensing systems, expanding the application range of wireless power supply sensing systems.

INDEX TERMS Anti-collision algorithm, sensing, wireless, passive, tag.

I. INTRODUCTION

With the development of science and technology, the Internet of Things (IoT) technology has gradually entered public life. Sensing technology, as one of the key technologies of the IoT, is the core to achieve the interconnection of everything in the IoT. Against the backdrop of the rapid development of the IoT, wireless sensor networks are also rapidly developing [1], [2]. At present, the power supply for wireless sensor networks is batteries, which makes it inconvenient to use and also brings drawbacks to practical applications. In response to this issue, current research mainly utilizes passive tags in RFID systems to achieve self power supply [3]. Wang et al. proposed a binary search tree algorithm based on physical layer network coding to improve the efficiency of multi tag recognition in RFID systems, reducing the number of interactions between readers and tags [4]. However, currently, the sensing tags and systems of wireless powered RFID systems also face problems, such as low efficiency, short communication distance, and low data throughput [5]. Based on these issues, a passive wireless low-power hydrogen concentration sensing system is designed. Dynamic clock frequency adjustment technology and self-excited deep sleep mechanism are introduced to reduce the power consumption of sensing tags. A dual capacitor energy collection and management circuit is designed. To further reduce the power consumption of sensing tags, a passive wireless magnetic field intensity sensing system is proposed to enhance sensing sensitivity. In response to the low efficiency in multi sensing tags, an efficient anti-collision algorithm based on dynamic binary query trees is developed. The collision and idle time slots are processed. A low-cost response mechanism is introduced into the algorithm. The research aims to solve the problems of existing wireless power supply sensing systems

The associate editor coordinating the review of this manuscript and approving it for publication was Alon Kuperman.

by designing multi angle and multi directional methods. It is expected to reduce the power consumption of sensing tags, improve the efficiency of multiple sensing tags, and promote the widespread application of wireless power supply sensing systems.

The contribution of the research lies in the design of two sensing systems and an anti-collision algorithm, which reduces the power consumption, error, energy collection rate of sensing labels, as well as the power consumption and total recognition time of anti-collision algorithms. This achieves leak free recognition and enhances the reliability of anti-collision algorithm recognition.

There are four innovative points in the research. Firstly, dynamic clock frequency adjustment technology and self excited deep sleep mechanism are introduced into the sensing system. Secondly, a multi base query tree is introduced into the anti-collision algorithm of the sensing system. Thirdly, multiple sensing systems are designed from multiple perspectives to address issues such as low power consumption or efficiency of sensing tags. Fourthly, a dual capacitor energy collection and management circuit is designed in the sensing system. The study is divided into four parts. The first part is a literature review related to wireless power supply sensing tags and systems. The second part is the design of research methods. The third part is the result analysis of the research method. The fourth part is the conclusion, shortcomings, and future prospects of the study.

II. RELATED WORKS

As the foundation for the perception layer of the IoT, wireless sensor networks can perceive, collect, and process information from different target objects through sensing tags. The working time of the sensing tags is limited by the capacity of the battery. Therefore, more scholars are conducting research on wireless power supply sensing tags and systems. Tuoi et al. designed a method that utilized thermo-electric generators to provide new power for wireless IoT sensing systems. This method converted the thermal energy generated by environmental temperature fluctuations into electrical energy. It was applied as a portable power source. In addition, this study evaluated the generation and storage of thermo-electric generators. When the ambient temperature fluctuation was closest to room temperature, the maximum output of the capacitor was 29μW [6]. To analyze the constant current/constant voltage performance of the multi coil electric vehicle radio energy transmission system under misaligned conditions, Luo et al. designed a resonant circuit compensation method based on an exciter orthogonal repeater transmitter. The orthogonal relay transmitter involved a small excitation coil and two decoupled orthogonal relay coils. These two types of coils were magnetically coupled. The experimental results showed that the system had higher efficiency, reaching 91.8% [7]. Samsami and Yasrebi designed an anti-collision algorithm based on Monte Carlo query tree search to solve the tag conflicts in RFID systems. The Monte Carlo query tree search method not only had the characteristics of traditional Monte Carlo tree search, but also had the ability to count queries. In addition, to verify the performance of the algorithm, the study analyzed the temporal and spatial complexity. The experimental results indicated that the method was significantly superior to existing methods in recognition efficiency [8]. To avoid the poor performance of the time division multiple access anti-collision algorithm when the number of labels was large, Jing et al. conducted simulation analysis on the performance of four anti-collision algorithms based on blind source separation. The experimental results showed that the fixed point algorithm was unstable [9].

Ai et al. designed an anti-collision algorithm based on time slot random regression binary search tree to avoid the unrecognizable tags caused by data collisions. This algorithm processed RFID tags through a regression binary search tree. In the same experimental conditions, the algorithm had higher efficiency and less time spent on recognition [10]. Xuan and Li designed an enhanced fast Q algorithm to improve the recognition efficiency of radio frequency identification systems. This algorithm considered the probability of conflicting time slots and idle time slots. The update rate of Q value was determined based on this probability and the duration of the time slot. In addition, the study also validated the effectiveness of the algorithm using discrete-time Markov chains. The experimental results showed that it had better performance compared to existing methods [11]. To improve the efficiency of RFID systems, Luo et al. proposed an anti-collision algorithm for an under-determined RFID hybrid system. This algorithm used non negative matrix factorization to achieve collision avoidance applications. Then it was integrated with the principle of tag independence. The experimental results showed that the method could effectively solve the under-determined collision problem and improve the efficiency of the radio frequency identification system [12]. Su et al. designed a binary splitting algorithm based on grouping to improve the recognition efficiency of ultra-high frequency radio frequency identification systems. This algorithm not only involved the optimal grouping strategy, but also included a label cardinality estimation method and an optimized binary splitting algorithm. The experimental results showed that the system throughput reached 0.48, which was significantly better than existing methods [13].

In summary, there is currently relatively rich research on wireless power supply sensing tags and systems. The anti-collision algorithms designed are also relatively diverse. However, there are still some problems with the current wireless power supply sensing system, such as low efficiency, low sensing sensitivity, and short communication distance. Therefore, a passive wireless low-power hydrogen concentration sensing system is innovatively proposed to reduce the power consumption of sensing tags. To further reduce the power consumption of sensing tags, a passive wireless magnetic field intensity sensing system is designed. In addition, to solve the low efficiency of multiple sensing

labels in wireless power supply sensing systems, an efficient anti-collision algorithm based on dynamic binary query trees is proposed.

III. WIRELESS POWER SUPPLY SENSING TAG AND SYSTEM DESIGN BASED ON ANTI-COLLISION ALGORITHM

In this chapter, to reduce the power consumption of sensing tags, a passive wireless low-power hydrogen concentration sensing system is designed. Dynamic clock frequency adjustment technology and self excited deep sleep mechanism are introduced into the system. To further reduce the power consumption of sensing tags, a passive wireless magnetic field intensity sensing system is designed. In response to the low efficiency of multiple sensing tags in wireless power supply sensing systems, an efficient anti-collision algorithm based on dynamic binary query trees is developed.

A. DESIGN OF PASSIVE WIRELESS LOW POWER HYDROGEN CONCENTRATION SENSING SYSTEM

In passive wireless identification systems, RF signals can be converted into DC energy to achieve self powered communication. The advantage of wireless power supply sensing tags and system is that they have a long usage time and basically do not require maintenance. It also makes the system have a relatively broad research prospect [14], [15]. However, there are also some issues with wireless power supply sensing systems at present, such as low data throughput, short communication distance, low sensing sensitivity, and low efficiency [16], [17]. Corresponding methods have been designed to address these issues. To reduce the power consumption of sensing tags and improve the data throughput of the sensing system, a passive wireless low-power hydrogen concentration sensing system is designed. Dynamic clock frequency adjustment technology and self-excited deep sleep mechanism are introduced to reduce the power consumption of sensing tag. A dual capacitor energy collection and management circuit is designed. To further reduce the power consumption of sensing tags in wireless power supply sensing systems, a passive wireless magnetic field intensity sensing system is designed to enhance sensing sensitivity. In response to the low efficiency in multi-sensing labels, an efficient anti-collision algorithm based on dynamic binary query trees is developed. The collision and idle time slots are processed. A low-cost response mechanism is introduced into the algorithm. The architecture of a passive wireless low-power hydrogen concentration sensing system is shown in Figure 1.

From Figure 1, the passive wireless low-power hydrogen concentration sensing system mainly involves routers, hydrogen concentration sensing tags, switches, monitoring computers, local computers, Ethernet connections, collectors, and Radio Frequency Identification (RFID) links. For the communication between the collector and the tag, the ISO/IEC 18000-6C protocol is adopted in the study. The main job of the collector is to obtain the hydrogen concentration

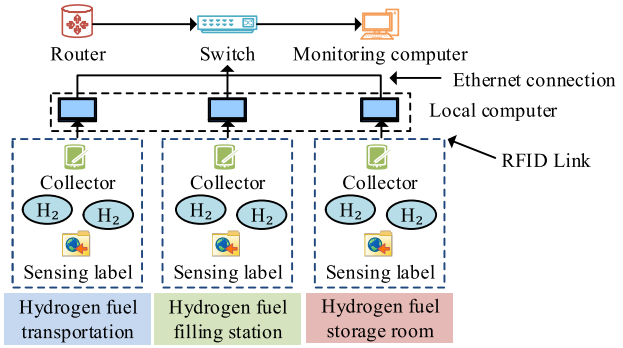

FIGURE 1. Architecture of passive wireless low power hydrogen concentration sensing system.

near the sensing tag, and then transmit it to the local computer. After passing through the switch, it is transmitted to the monitoring computer. To obtain the concentration of hydrogen gas, the extended Read command in the RFID protocol is used to represent it. For label selection, the study uses the Select command, which can avoid multiple tag recognition. In addition, data collection commands also use fixed link parameters. The overall circuit architecture of the passive wireless low-power hydrogen concentration sensing tag includes an antenna that converts RF energy into DC energy, matching circuit, power divider, and rectifier circuit. In addition, the circuit architecture of the sensing tag also involves modulation circuits and signals, low voltage differential linear regulators, base-band signal processing circuits, hydrogen sensors and signal conditioning circuits, energy collection and management circuits, energy storage capacitors, and demodulation circuits that include detection, low-pass, and comparison. By collecting and managing energy, the active circuit of the tag can be powered. For the implementation of energy collection and management, the BQ25570 chip is usually used. However, the circuit structure of BQ25570 is very complex and its size is large, making it difficult to apply to label chips [18]. Therefore, a dual capacitor energy collection and management circuit is designed to improve the energy collection rate. To achieve energy collection and management, this circuit fully utilizes the different charging and discharging characteristics of the energy collection circuit and control circuit. Then it is combined with solar cells to connect the output terminals of the battery and rectifier circuit in parallel to BQ25570. In addition, the energy collection and management circuit also includes energy storage circuits, output and energy-saving control circuits. By setting the component parameter values in these circuits, different application requirements can be met. To reduce tag power consumption, a Micro Controller Unit (MCU) is used in the study. The operating voltage of the MCU is 2V. In addition, the study also considers MCU as a way to achieve functional control of RFID protocol. To reduce tag power consumption, efficient assembly language and dynamic clock frequency adjustment technology are adopted in the study. Dynamic clock frequency adjustment technology can set different main

clock frequencies for different modules. It can reduce the power consumption of tags. In addition, dynamic clock frequency adjustment technology can also reduce circuit heat dissipation and extend the lifespan of the circuit [19], [20]. To further reduce the average power consumption of tags, a self excited deep sleep mechanism is designed. This mechanism can not only reduce the average power consumption of each label in a multi label system, but also improve the data throughput of the multi label system [21]. This sleep mechanism is applied to the engineering process of sensing tags, indicating that collector commands are not processed. Through this mechanism, tags can be implemented without other functions during the deep sleep phase. The operating principle of this mechanism is as follows. When no tag selection is made or the work is completed, all peripheral circuit power will be turned off by the MCU and enter deep sleep mode. The workflow of sensing tags is shown in Figure 2.

FIGURE 2. The workflow of sensing labels.

From Figure 2, the workflow of sensing tags mainly consists of five stages. The first stage is the deep dormancy stage. At this stage, no processing is performed on the collector commands. The second stage is the low-power detection stage. The third stage is the command analysis stage. The fourth stage is the data collection stage. The fifth stage is the data transmission stage. At different stages, tags can collect energy. The stage with the highest charging efficiency is the deep sleep stage. The structural content of implementing the ISO/IEC 18000-6C protocol through MCU mainly includes decoding and encoding module, command execution module, memory module, random number generator module, finite state machine module, and clock configuration module. Among them, the reduction of MUC power consumption is mainly achieved through the clock configuration module. In the interrupt program, the length of the received symbol is shown in equation (1) [22].

$$Len\_re = Number\_reg / f_{clk}^{cal} \tag{1}$$

In equation (1), f_{clk}^{cal} represents the clock frequency of the counter module. $Number\_reg$ represents the value of the currently recorded counter. In the structure of a hydrogen concentration sensor, the output voltage is shown in equation (2) [23].

$$V_{AB} = V_{power} \frac{R_{s1}R_{s2} - R_2R_1}{(R_1 + R_{s1})(R_2 + R_{s2})} \tag{2}$$

In equation (2), V_{AB} represents the output voltage of the bridge. V_{power} is the output voltage. R_1 and R_2 represent sliding rheostats. R_{s1} and R_{s2} represent the resistance values of the hydrogen sensing element. To more accurately sense hydrogen concentration, a fitting function for hydrogen concentration is established, as shown in equation (3).

$$HC = f(V_{ADC}) \approx f_{HC}(V_{ADC}) \tag{3}$$

In equation (3), V_{ADC} represents voltage. HC represents the concentration of hydrogen gas. $f_{HC}(V_{ADC})$ is the fitting function. To address the voltage being easily affected by temperature, the research adopts the temperature compensation. The fitting function after temperature compensation is shown in equation (4).

$$HC = f(V_{ADC}) \approx f_{HC}\left(V_{ADC}^{T}\right) \approx f_{HC}\left(\frac{V_{ADC}}{f_{factor}^{V_{ADC}}(T)}\right) \tag{4}$$

In equation (4), V_{ADC}^{T} represents the voltage value after temperature compensation. T represents temperature, in degrees Celsius. $f_{factor}^{V_{ADC}}(T)$ is the fitting function after temperature compensation. To reduce the charging time of different tags and improve the data throughput of the sensing system, a tag charging time prediction model is designed. This model can predict tag charging time based on the number of tags, energy consumption, and distance from the collector. The prediction model for tag charging time is shown in equation (5).

$$T_{ch} = -\Pi_R \ln\left(1 - \left(v_{bat}(\Upsilon) - V_{bat,0}^{N_{tag}}\right) / \left(V_h - V_{bat,0}^{N_{tag}}\right)\right) \tag{5}$$

In equation (5), $-\Pi_R$ represents the time charging constant. $v_{bat}(\Upsilon)$ represents the charging formula when capacitor C_{bat} has an initial voltage $V_{bat,0}$. V_h represents the highest voltage that capacitor C_{bat} can reach. $V_{bat,0}^{N_{tag}}$ represents the voltage in the capacitor C_{bat} after the label is working. The label energy collection efficiency is shown in equation (6).

$$EnergyCollectionEfficiency = \frac{1}{2}\frac{C_{bat}V_{bat}^2}{P_{tag}T_{ch}} \times 100\% \tag{6}$$

In equation (6), P_{tag} represents the power received by the tag. T_{ch} is the tag charging time prediction model. V_{bat} represents the charging threshold voltage. C_{bat} represents the label energy storage capacitor.

The efficiency of sensing systems can be defined by multiple parameters, such as label power consumption and distance. The average power consumption for each tag in the sensing tag is shown in equation (7).

$$\text{Average Power} = \frac{P_A + \frac{P_A}{2} \times (N_{tag} - 1)}{N_{tag}} \tag{7}$$

In equation (7), P_A represents the power consumption of the activation mode. N_{tag} represents the number of tags. The average power consumption of the sensing system is shown in equation (8).

$$\text{Average Power system} = \frac{P_A + \frac{P_A}{2} \times \frac{N_{tag}}{2}}{N_{tag}} \tag{8}$$

The calculation of energy collection rate is to divide the collected energy by the charging time, in mJ/s.

B. DESIGN OF PASSIVE WIRELESS MAGNETIC FIELD INTENSITY SENSING SYSTEM

In a passive wireless low-power hydrogen concentration sensing system, continuous activation of the MCU bringssome power consumption. Therefore, there is room for further improvement in the system. The offset frequency within the range is much smaller than the frequency of the output center of the resonant magnetic field intensity sensor. Therefore, the direct measurement of sensor output frequency method enhances the power consumption of the measurement. In addition, in reducing the center frequency, the sensitivity of a single sensor in the method of mixing the sensor output signal with the reference clock signal is also lower [24], [25]. Therefore, to further reduce the power consumption of sensing tags in wireless power supply sensing systems and enhance sensing sensitivity, a passive wireless magnetic field intensity sensing system is designed. The architecture of the passive wireless magnetic field intensity sensing system is shown in Figure 3.

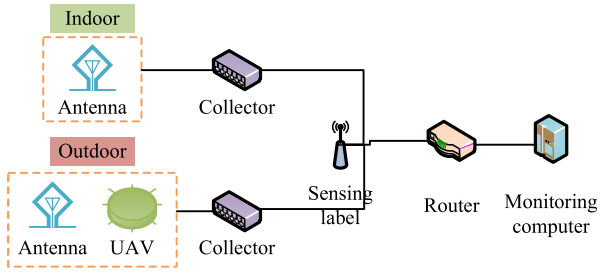

FIGURE 3. Architecture of passive wireless magnetic field strength sensing system.

From Figure 3, the architecture of the passive wireless magnetic field intensity sensing system involves antennas, collectors, routers, drones, monitoring computers, and magnetic field intensity sensing tags. The application scenarios mainly involve indoor household appliances and outdoor power transmission systems. A passive wireless dual resonant magnetic field intensity sensing tag and system is designed for indoor household appliances. To reduce tag power consumption, the sensing data in the sensing system uses an analog transmission mechanism. The tag uses RF energy for power supply. In addition, the system is designed based on the exclusive-or gate detection circuit. In the exclusive-or gate detection circuit, the Fourier transform of square wave signals $x_1(t)$ and $x_2(t)$ generated by two sensors is shown in equation (9) [26].

$$\begin{cases} F[x_1(t)] = 2\tau_1\omega_1\delta(\omega) + X_1(\omega) \\ F[x_2(t)] = 2\tau_2\omega_2\delta(\omega) + X_2(\omega) \end{cases} \tag{9}$$

In equation (9), $2\tau_1$ and $2\tau_2$ represent the pulse widths of $x_1(t)$ and $x_2(t)$, respectively. ω_1 and ω_2 represent the angular frequencies of $x_1(t)$ and $x_2(t)$, respectively. $X_1(\omega)$ represents the spectrum of the alternating current component in $x_1(t)$. $X_2(\omega)$ is the spectrum of the alternating current component in $x_2(t)$R. $\delta(\omega)$ represents the transformation of diagonal frequency. The Fourier transform of the exclusive-or gate output signal is shown in equation (10) [27].

$$F(x_1(t) \odot x_2(t)) = \pi\delta(\omega) - \frac{1}{\pi}X_1(\omega) \otimes X_2(\omega) \tag{10}$$

In equation (10), $\odot$ represents the exclusive-or operation. $\otimes$ represents convolution. The frequency signal generated by $X_1(\omega)$ and $X_2(\omega)$ convolution is shown in equation (11).

$$\begin{aligned} &X_1(\omega) \otimes X_2(\omega) \\ &\quad = 4[\delta(\omega - (\omega_1 - \omega_2)) + \delta(\omega - (\omega_2 - \omega_1))] \end{aligned} \tag{11}$$

In equation (11), ω represents the angular frequency. The circuit architecture of the passive wireless dual resonant magnetic field intensity sensing tag is shown in Figure 4.

From Figure 4, the circuit architecture of the passive wireless dual resonant magnetic field intensity sensing tag mainly involves antennas, power splitters, modulation circuits, demodulation circuits, energy collection and management, MCU, dual sensors, driving circuits, XOR gate sensing circuits, rectification circuits, collectors, selectors, and two low-voltage differential linear regulators. The modulation circuit includes two sets of N-Metal-Oxide-Semiconductor (NMOS) transistors. The energy collection and management in this sensing tag also adopts the dual capacitor energy collection and management circuit in the passive wireless low-power hydrogen concentration sensing tag. It fully utilizes the different charging and discharging characteristics of the energy collection circuit and control circuit to achieve energy collection and management. This sensing tag can not only perform single sensor sensing, but also dual sensor sensing. In addition, the working mode of the tag is controlled by extending the parameters of the Read command. The working path of the passive wireless dual resonant magnetic field intensity sensing tag is shown in Figure 5.

From Figure 5, the first step in the passive wireless dual resonant magnetic field intensity sensing tag is to initialize the MCU, select the sensor mode, and turn off the low voltage differential linear regulator. The second step is to detect the demodulated signal. The third step is to determine whether the sensor mode command is received. If the command is in single sensor mode, the first low pressure differential linear regulator is opened, the duration is calculated, a single sensor is selected, and the signal is responded to and then terminated. If the command is in dual sensor mode, two low-pressure differential linear regulators are opened to calculate the duration. The signal is responded to and counted. If the third step does not receive the command, the traditional RFID is implemented through enter the traditional mode. Finally, the process is ended.

C. DESIGN OF ANTI-COLLISION ALGORITHM FOR MULTI-SENSING TAGS

At present, there are some problems with wireless power supply sensing systems, such as low data throughput, short communication distance, low sensing sensitivity, and low efficiency. A corresponding sensing system is

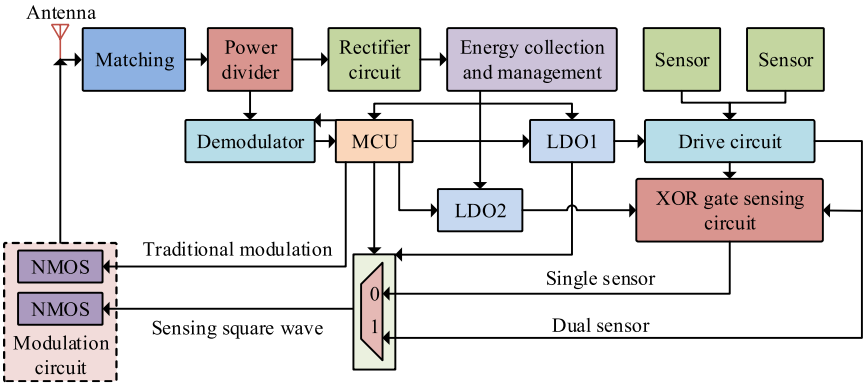

FIGURE 4. The circuit architecture of passive wireless double resonant magnetic field strength sensing label.

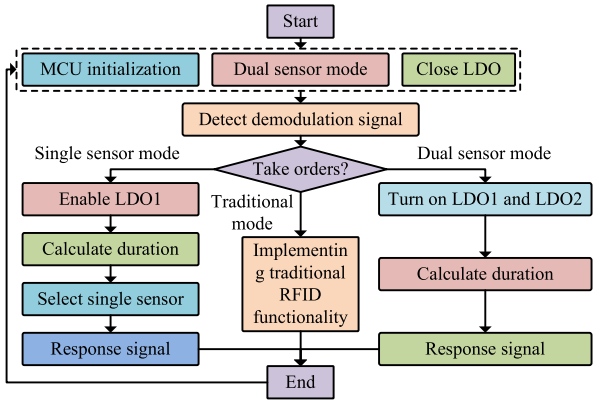

FIGURE 5. The working path of passive wireless double resonant magnetic field strength sensing tag.

designed to address issues such as low data throughput and power consumption. To solve the low efficiency of multi-sensing tags, an efficient anti-collision algorithm based on Dynamic Multi-base Query Tree (DMQT) is designed. This anti-collision algorithm aims to improve the efficiency of tag access, reduce system complexity, and solve the tag access failure caused by capture effects. Among existing anti-collision algorithms, some rely heavily on tag quantity estimation algorithm, which also leads to high complexity in algorithm design, such as the algorithm based on the Aloha mechanism. Some algorithms may have more collisions or idle time slots, such as the algorithm based on tree structure [28], [29]. In addition, there are many anti-collision algorithms that have not taken into account the impact of capture effects on tag recognition, resulting in tags that cannot be accessed by collectors [30], [31]. To avoid these problems, the efficient collision prevention algorithm based on DMQT is developed, taking into account the total collision bit. Collision time slots and idle time slots are processed. A low-cost response mechanism is introduced in DMQT. In addition, DMQT does not need to consider label quantity estimation algorithms, which can reduce recognition time and energy consumption [32]. The energy collection rate is achieved by dividing the collected energy by the charging time. The DMQT eliminates idle and collision time slots, reducing the time and energy consumption of accessing a single tag. Therefore, this algorithm can improve the energy collection rate.

Through collision information detection technology, the number of collision positions and the collision positions can be determined. This technology is usually based on Manchester encoding [33], [34]. To improve the recognition efficiency of efficient collision prevention algorithms based on DMQT, the study fully utilizes all collision bits. The first involved is the dynamic query prefix acquisition mechanism, which obtains collision information through Manchester encoding. Then this mechanism is used to calculate the collision bits that need to be processed. Secondly, the collision information mapping mechanism is involved. The key to this mechanism is that the collector needs to generate Map commands. Finally, the multi label query mechanism is involved. The collector needs to generate a Query command. In the temporal logic of DMQT, all Map commands and Query commands correspond one-to-one, except for the first Map command. The m collision positions are shown in equation (12) [35].

$$m = \begin{cases} 1, & if \ \left(\left\lfloor \log_n (L) \right\rfloor\right) = 0 \\ \left\lfloor \log_n (L) \right\rfloor, & otherwise \end{cases} \tag{12}$$

In equation (12), n represents a variable parameter. L represents the total number of collision bits received by the collector, with the maximum value of ID_length. In the collision information mapping mechanism, the m collision bits $Z\_bit_k^{reader}$ of the original label in group U is shown in equation (13).

$$Z\_bit_k^{reader} = dec2bin\left(p_k^{(Q)}, \alpha\right), \quad k \in \{1, \ldots, U\} \tag{13}$$

In equation (13), $p_k^{(Q)}$ represents the corresponding position of the collision bit. α represents the total number of bits converted to binary. Q represents the Query command. k is the serial number of the group. $dec2bin$ is a mathematical function that converts decimal digits into binary digits. In the

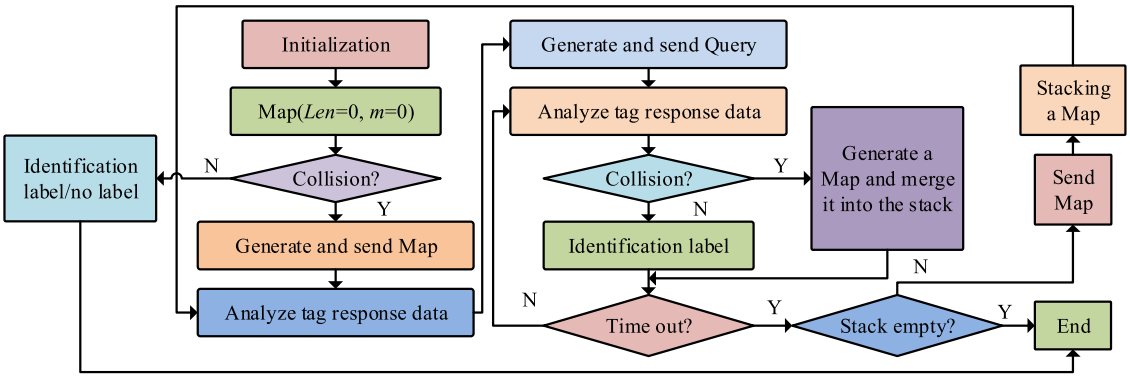

FIGURE 6. The main process of DMQT anti-collision algorithm.

multi label query mechanism, the new matching information *Info* is shown in equation (14) [36].

$$Info^{(new)} = \left\{ Info^{(old)}, Info^{(rem)} \right\} \tag{14}$$

In equation (14), $Info^{(old)}$ represents the matching information generated by the previous Map command. $Info^{(rem)}$ represents the matching information generated based on the remaining Identity Document (ID). The new matching information length *Len* is shown in equation (15).

$$Len^{(new)} = Len^{(old)} + Len_{Info}^{(rem)} \tag{15}$$

In equation (15), $Len^{(old)}$ represents the length of matching information generated by the previous Map command. $Len_{Info}^{(rem)}$ represents the length of matching information generated based on the remaining ID. The delayed response time is shown in equation (16) [37].

$$\partial_{delay,i} = \partial_1 + \left(\partial_3 + \partial_\beta\right)(i-1) \tag{16}$$

In equation (16), i represents the sub time slot. ∂_1 represents the response time of the tag. ∂_3 is the interval time between tag responses in adjacent sub time slots in the Query command. ∂_β represents the duration of the response signal returned by the tag. The total time to execute the Query command is shown in equation (17).

$$\partial_{Query}^{all} = \partial_1 + \eta\left(\partial_3 + \partial_\beta\right) + \partial_2 - \partial_3 \tag{17}$$

In equation (17), ∂_2 represents the response time of the collector. η represents the total number of sub time slots. The main process of the DMQT anti-collision algorithm is shown in Figure 6.

From Figure 6, the first step of the DMQT anti-collision algorithm is initialization. The second step is to send the Map command ($Len = 0, m = 0$). The third step is to determine whether the collision exists. If it does not exist, the tag will be identified and the process will end after identifying the tag. If it exists, a Map command ($Len = 0, m \neq 0$) is generated and sent. The fourth step is to analyze the tag response data. The fifth step is to generate and send Query commands. The sixth step is also to analyze the tag response data. The seventh step is to determine whether the collision exists again. If it does not exist, the label will be identified. Otherwise, a Map command will be generated and incorporated into the process. The eighth step is to determine whether the timeout has occurred. If it is true, the process is returned to step six. Otherwise, proceed to step nine. The ninth step is to determine the stack. If it is determined to be yes, the process is ended. If it is determined to be no, a Map command needs to be given, followed by sending the Map command ($Len \neq 0, m \neq 0$). Finally, the process is returned to step four. In the tag recognition, the DMQT anti-collision algorithm utilizes a dynamic multi-digit query tree. The structure of the multi-digit query tree is shown in Figure 7 [38], [39].

In Figure 7, H represents the number of layers in the query tree. H_0 represents the initial layer. H_1 and H_2 represent the first and second layers, respectively. H_{Max} represents the theoretical maximum number of layers in the query tree. ε is a fixed value. The average number of collisions required to identify a single tag is shown in equation (18).

$$\mathrm{E}_{avg} = \Im\left(E_{\theta_{tag}}\right)/\theta_{tag} \tag{18}$$

In equation (18), $\Im\left(E_{\theta_{tag}}\right)$ represents the expected number of collision nodes. θ_{tag} represents the number of different labels. To address the missing recognition caused by capture effects, the study introduces an Ack command on DMQT. It is used to indicate tag recognition. In addition, the Ack command does not require a return response signal for the tag.

IV. RESULT ANALYSIS OF WIRELESS POWER SUPPLY SENSING TAG AND SYSTEM

In this chapter, the performance of hydrogen concentration sensing tags and systems is analyzed. The main analysis content includes the charging time of labeled energy storage capacitors under cold start and hot start, performance comparison of different sensing tags, and performance verification of the tag charging time prediction model. In addition, the study analyzes the resonant magnetic field intensity sensing

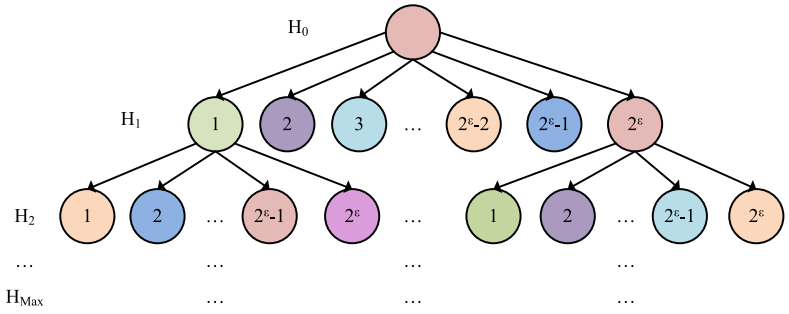

FIGURE 7. The structure of a multi-digit query tree.

tags and systems. The performance of the DMQT based anti-collision algorithm is also verified.

A. RESULT ANALYSIS OF HYDROGEN CONCENTRATION SENSING TAG AND SYSTEM

To analyze the energy collection performance of hydrogen concentration sensing tags, the charging time of tag energy storage capacitors under cold and hot start conditions is analyzed. Performance testing platforms are built both indoors and outdoors for the experiment, including antennas, collectors, labels, and multi-meter. The outdoor testing platform also has absorbing materials. The collector in the testing platform uses an 8dBi circularly polarized antenna, with an equivalent isotropic radiation power of 36dBm. The output frequency of the signal generator is set to 935MHz. The power varies within the range of −20dBm to 14dBm. The model of the multi-meter is Fluke 17B. The energy collection performance test results of the hydrogen concentration sensing tag were shown in Figure 8.

From Figure 8 (a), when the distance between the outdoor collector and the tag was 3m, the voltage of the energy storage capacitor also increased with the increase of cold start charging time. When the cold start charging time was less than 60s, the voltage growth of the energy storage capacitor was relatively slow. When the cold start charging time exceeded 60s, the growth rate of energy storage capacitor voltage suddenly increased. When the cold start charging time reached 85s, the growth rate of the energy storage capacitor voltage became flat. The maximum voltage of the energy storage capacitor was 5.25V. In Figure 8 (b), the charging time for both indoor and outdoor cold start and hot start increased with the distance between the collector and the tag. The maximum value of cold start charging time indoors was 152s and the minimum value was 0s. The maximum value of hot start charging time was 48s, and the minimum value was 0s. The maximum outdoor cold start charging time was 398s, and the minimum value was 0s. The maximum value of hot start charging time was 98s, and the minimum value was 0s. From this, when the distance between the collector and the label was the same, the indoor charging time was significantly shorter than the outdoor charging time. The cold start charging time was much

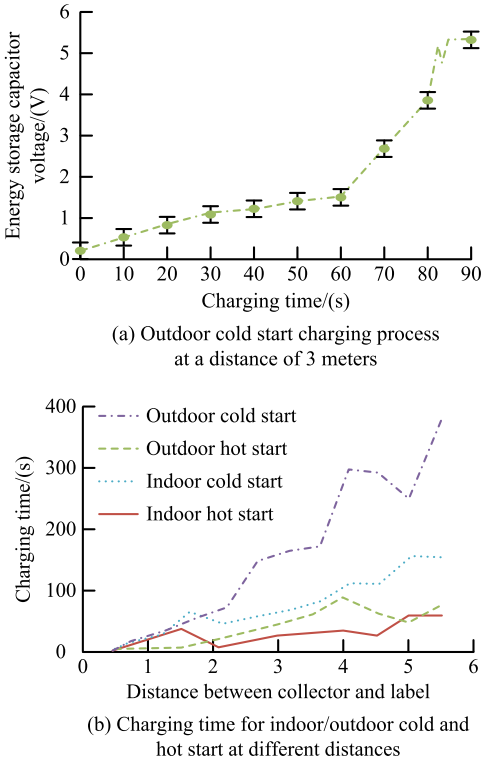

FIGURE 8. Hydrogen concentration sensing label energy collection performance test results.

longer than the hot start charging time. To better validate the wireless energy collection performance of the sensing tags, similar designs from references [40] and [41] were selected for comparison. Reference [40] was a wireless sensor that could achieve self powered energy collection, while reference [41] designed a miniaturized RFID tag sensor. At this point, the distance between the label and the collector was 2m. The performance comparison results were shown in Table 1.

From Table 1, in the cold start indoor environment, the energy collection rate of the sensing tag designed in the research was 0.081mJ/s, and the energy collection efficiency was 25.7%. The energy collection rate of the self powered energy collection wireless sensor sensing tagwas

TABLE 1. Comparative results of wireless energy harvesting performance.

Start mode	Setting	Method	Collected energy	Charging time	Energy collection rate(mJ/s)	Received by tag Power(dBW)	Energy collection efficiency
Cold start	Indoor	Compact energy harvester	2.9mJ	39s	0.074	0.402	18.5%
		Miniaturized RFID tag sensor	3.7mJ	187s	0.020	0.238	8.3%
		Research	5.0mJ	62s	0.081	0.317	25.7%
	Outdoor	Compact energy harvester	2.9mJ	92s	0.032	0.362	8.7%
		Miniaturized RFID tag sensor	3.7mJ	209s	0.018	0.277	6.4%
		Research	5.0mJ	94s	0.053	0.532	10.0%
Hot start	Indoor	Compact energy harvester	2.6mJ	28s	0.093	0.348	26.7%
		Miniaturized RFID tag sensor	25mJ	129s	0.193	0.433	44.8%
		Research	4.6mJ	16s	0.288	0.490	58.7%
	Outdoor	Compact energy harvester	2.6mJ	67s	0.039	0.196	19.8%
		Miniaturized RFID tag sensor	25mJ	187s	0.134	0.552	24.2%
		Research	4.6mJ	30s	0.153	0.401	38.2%

0.074mJ/s, and the energy collection efficiency was 18.5%. The energy collection rate of the miniaturized RFID tag sensor sensing tag was 0.020mJ/s, and the energy collection efficiency was 8.3%. In the cold start outdoor environment, the energy collection rates of the three sensing tags were 0.053mJ/s, 0.032mJ/s, and 0.018mJ/s, respectively, with energy collection efficiency of 10.0%, 8.7%, and 6.4%. In the hot start indoor environment, the energy collection rates of the three sensing tags were 0.288mJ/s, 0.093mJ/s, and 0.193mJ/s, respectively, with energy collection efficiency of 58.7%, 26.7%, and 44.8%. In the hot start outdoor environment, the energy collection rates of the three sensing tags were 0.153mJ/s, 0.039mJ/s, and 0.134mJ/s, respectively, with energy collection efficiency of 38.2%, 19.8%, and 24.2%. From this, the sensing tags designed in the research had better performance and significant advantages inenergy collection rate and efficiency. To verify the performance of the tag charging time prediction model, a testing platform was constructed, which mainly involved tag groups, antennas, collectors, and oscilloscopes. The comparison between tag prediction and actual charging time required in indoor and outdoor environments was shown in Figure 9.

From Figure 9 (a), in the indoor environment, when the tags were 20, the predicted charging time was basically consistent with the actual test charging time. When the distance between the collector and the tag exceeded 4m, there was a significant deviation between the predicted charging time and the actual test charging time. The maximum predicted charging time was 7s, and the actual maximum tested charging time was 34s. When the tags were 60, the predicted charging time and actual test charging time were roughly consistent. When the distance between the collector and the tag exceeded 3.5m, there was a significant deviation between the predicted charging time and the actual test charging time. The maximum predicted charging time was 19s, and the actual test charging time was 61s. The difference between the two was 42s. From Figure 9 (b), in the outdoor environment, when the tags were 20, the maximum predicted charging time was 20s, and the actual maximum tested charging time was 58s. When the

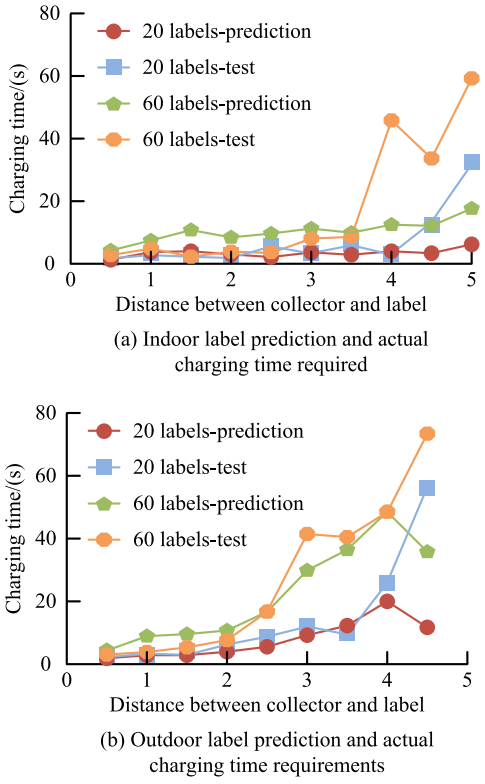

FIGURE 9. Comparison of label prediction and actual charging time required in indoor and outdoor environments.

distance between the collector and the tag exceeded 3.5m, there was a deviation between the predicted charging time and the actual test charging time. When the tags were 60, the maximum predicted charging time was 51s, and the actual maximum tested charging time was 72s. When the distance between the collector and the tag exceeded 4m, there was a significant deviation between the predicted charging time and the actual test charging time. In most cases, the predicted charging time and actual test charging time were basically consistent, indicating that the tag charging time prediction model had good performance.

B. RESULT ANALYSIS OF PASSIVE WIRELESS MAGNETIC FIELD INTENSITY SENSING SYSTEM

To analyze the performance of the resonant magnetic field intensity sensing tag and system, the sensing error of the static magnetic field was measured. In the testing environment, two resonant magnetic field strength sensors are installed in the sensors. The magnetic field data is obtained by calibrating the sensing labels. The equipment required for calibration includes signal generators, sensing tags, and collectors. The frequency of the signal generator was 52Hz. The magnetic field intensity around the label is set to 25mT. The equivalent isotropic radiation power is 36dBm. In the test, the cable current was between 0.4A and 52A. All frequencies corresponding to the current were collected through a collector. The error comparison of sensing static magnetic field under different sensor modes was shown in Figure 10.

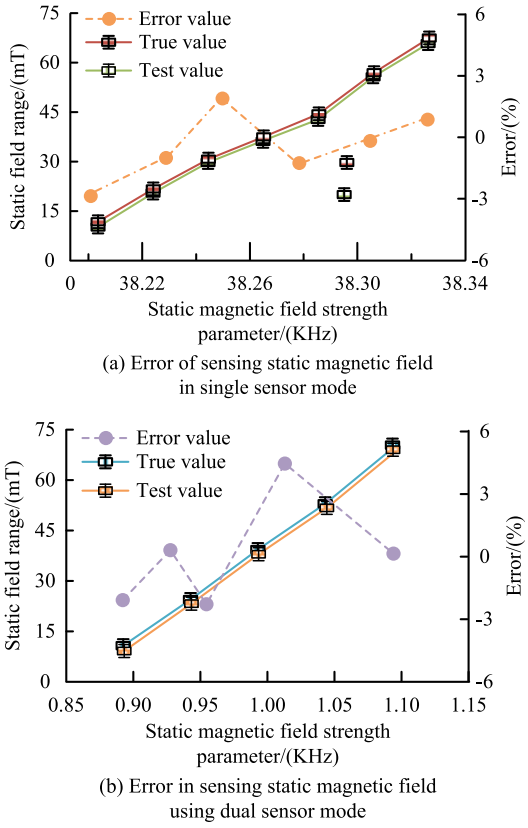

FIGURE 10. Error comparison of static magnetic field sensed by different sensor modes.

In Figure 10 (a), in the single sensor mode, the maximum value of sensing error was 2.1% and the minimum value was −2.8%. The maximum value of the static magnetic field sensing value and the true value were 74.7 and 74.6, respectively. The minimum values were 14.8 and 14.6, respectively. From Figure 10 (b), in the dual sensor mode, the maximum value of sensing error was 5.2% and the minimum value was −2.7%. The maximum value of the static magnetic field sensing value and the true value were 74.8 and 74.7, respectively. The minimum values were 14.8 and 14.6, respectively. Under different sensor modes, the error in sensing the static magnetic field was less than 5.5%, which also indicated that the resonant magnetic field intensity sensing tag and system had good performance. To verify the communication performance of the sensing tag and system, a communication performance testing platform was constructed. This testing platform involved antennas, collectors, absorbing materials, signal generators, power amplifiers, tags, ammeters, and magnetometers. The collector still used an 8dBi circularly polarized antenna. To avoid repeated testing, this study only conducted experiments on single sensor modes. The test results were shown in Figure 11.

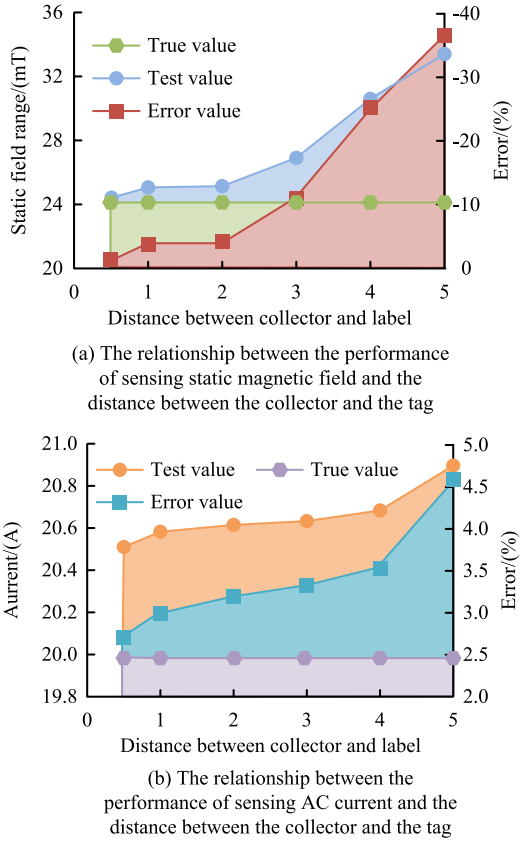

FIGURE 11. Communication performance test results of sensing tags and systems.

In Figure 11 (a), the maximum value of the static magnetic field sensing value was 34.2mT and the minimum value was 24.1mT. The maximum and minimum values of the true value in the static magnetic field were both 24mT. As the distance between the collector and the tag increased, the sensing value of the static magnetic field also gradually increased. The true value of the static magnetic field remained basically unchanged. From Figure 11 (b), the maximum value of the electric influenza sensing value was 20.93A, and the minimum value was 20.54A. The maximum and minimum values of the true current value were both 20A. As the distance between the collector and the tag increased, the current

sensing value also gradually increased, and the actual current value remained basically unchanged. As the distance between the collector and the tag increased, the static magnetic field sensing error also increased, and the current sensing value error also gradually increased. The static magnetic field sensing error and current sensing value error were relatively small, which also indicated that the resonant magnetic field intensity sensing tag and system had good communication performance.

C. SIMULATION VERIFICATION OF ANTI-COLLISION ALGORITHM BASED ON DMQT

To verify the performance of the anti-collision algorithm based on DMQT, other anti-collision algorithms were selected for experiments. The experimental environmentis a Windows 10(64 bit) operating system, with an Intel Core i5 13500H processor. The central processing unit is 2.6GHz, the memory is 64GB, and the core graphics card is Intel Iris Xe Graphics 80EU. The indicators for comparison includes total recognition time and energy consumption. A total of 5 experiments are conducted. The comparison algorithms include Dynamic Frame Slotted Aloha (DFSA) algorithm, Q-value algorithm, Slotted Aloha Regression Binary Search Tree (SA-RBST) algorithm, and Monte Carlo Query Tree Search (MCQTS) algorithm. The total recognition time and energy consumption were shown in Figure 12.

From Figure 12 (a), the maximum recognition time based on the DMQT anti-collision algorithm was 2.78s, and the minimum value was 1.31s. The maximum recognition time of the Q-value algorithm was 7.98s, and the minimum value was 5.46s. The maximum recognition time of the DFSA algorithm was 13.48s, and the minimum value was 9.76s. The maximum recognition time of the MCQTS algorithm was 8.07s, and the minimum value was 4.87s. The maximum total recognition time of the SA-RBST algorithm was 7.45s, and the minimum value was 5.03s. In Figure 12 (b), the maximum energy consumption based on the DMQT anti-collision algorithm was 4.71mJ and the minimum value was 3.21mJ. The maximum energy consumption of the Q-value algorithm was 8.73mJ, and the minimum value was 6.58mJ. The maximum energy consumption of the DFSA algorithm was 16.72mJ, and the minimum value was 12.36mJ. The maximum energy consumption of the MCQTS algorithm was 7.99mJ, and the minimum value was 6.02mJ. The maximum energy consumption of the SA-RBST algorithm was 7.98mJ, and the minimum value was 5.21mJ. The anti-collision algorithm based on DMQT outperformed the other two comparison algorithms in terms of total recognition time and energy consumption, indicating that the anti-collision algorithm based on DMQT had good performance. To further validate the performance of the DMQT based anti-collision algorithm, the accuracy and Mean Squared Error (MSE) were selected for comparison in the study. The experimental environment remained unchanged. The number of experiments was 4. The accuracy and MSE were shown in Table 2.

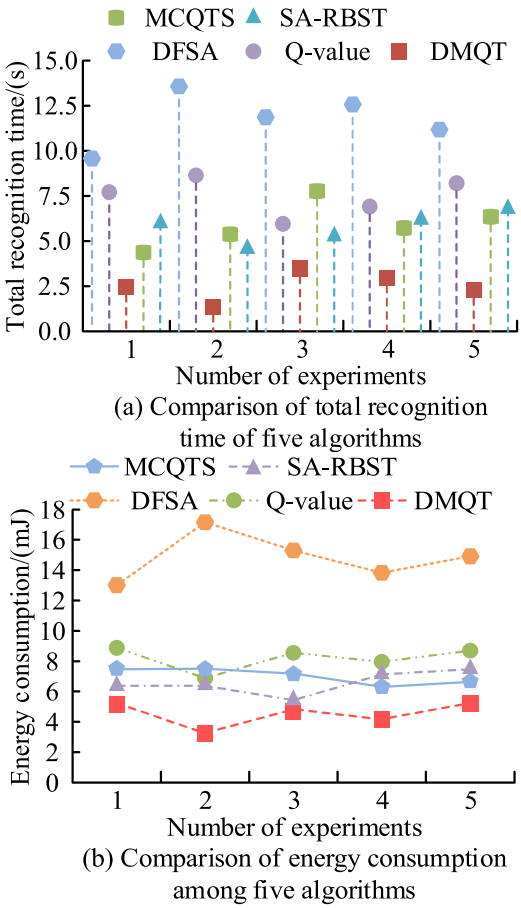

FIGURE 12. Comparison of total recognition time and energy consumption of three algorithms.

From Table 2, the maximum accuracy of the anti-collision algorithm based on DMQT was 99.36%, and the minimum accuracy was 97.11%. The maximum accuracy of the DFSA was 91.28%, and the minimum value was 89.31%. The maximum accuracy of the Q-value algorithm was 95.62%, and the minimum value was 93.89%. The maximum accuracy of the MCQTS algorithm was 97.36%, and the minimum value was 95.82%. The maximum accuracy of the SA-RBST algorithm was 97.79%, and the minimum value was 96.27%. The maximum MSE value based on the DMQT was 0.371 and the minimum value was 0.237. The maximum MSE value of the DFSA algorithm was 1.377, and the minimum value was 0.976. The maximum MSE of the Q-value algorithm was 0.652, and the minimum value was 0.553. The maximum MSE value of the MCQTS algorithm was 0.468, and the minimum value was 0.397. The maximum MSE of the SA-RBST algorithm was 0.479, and the minimum value was 0.388. The performance of the DMQT anti-collision algorithm was significantly superior to the comparison algorithms. To verify the performance of the DMQT algorithm, a comparison is conducted on the time and energy consumption of the algorithm in identifying different numbers of labels. Comparison algorithms include DFSA, Q-value, MCQTS, and SA-RBST. The number of iterations for the DMQT algorithm

TABLE 2. Comparison of the precision and MSE values of the three algorithms.

Algorithm	Precision				MSE			
	Number of experiments				Number of experiments			
	1	2	3	4	1	2	3	4
DMQT	98.55%	97.11%	99.36%	97.91%	0.371	0.368	0.276	0.237
DFSA	89.31%	90.74%	91.28%	89.76%	0.976	1.377	1.065	1.271
Q-value algorithm	95.62%	94.74%	93.89%	94.88%	0.652	0.553	0.624	0.593
MCQTS	96.77%	95.82%	97.36%	96.33%	0.468	0.421	0.397	0.403
SA-RBST	97.25%	96.58%	97.79%	96.27%	0.479	0.466	0.435	0.388

TABLE 3. Comparison of label recognition time and energy consumption of different algorithms.

Algorithm	Recognition time(s)				Energy consumption(mJ)			
	Number of tags				Number of tags			
	400	800	1200	1600	400	800	1200	1600
DMQT	0.52	1.12	1.98	2.01	1.381	1.237	1.275	1.301
DFSA	1.37	3.21	3.48	4.83	2.612	2.534	2.468	2.409
Q-value	1.56	3.38	4.07	5.62	2.987	2.912	2.935	2.976
MCQTS	0.83	1.93	2.24	3.12	2.132	2.239	2.067	1.996
SA-RBST	0.86	1.98	2.37	3.25	2.145	2.433	2.155	2.004

is set to 1200. The variable parameter n is set to 2.2. The values for the number of labels are 400, 800, 1200, 1600, and 2000, respectively. The label recognition time and energy consumption for different algorithms are shown in Table 3.

From Table 3, the maximum recognition time of the DMQT algorithm was 2.01s, and the minimum value was 0.52s. The maximum recognition time of DFSA algorithm and Q-value algorithm was 4.83s and 5.62s respectively, and the minimum value was 1.37s and 1.56s, respectively. The maximum recognition time of MCQTS algorithm and SA-RBST algorithm was 3.12s and 3.25s, respectively, and the minimum value was 0.83s and 0.86s, respectively. The maximum energy consumption of the DMQT algorithm was 1.381mJ, and the minimum value was 1.237mJ. The maximum energy consumption of DFSA algorithm, Q-value algorithm, MCQTS algorithm, and SA-RBST algorithm was 2.612mJ, 2.987mJ, 2.239mJ, and 2.433mJ, respectively, while the minimum values were 2.409mJ, 2.912mJ, 1.996mJ, and 2.004mJ, respectively. From this, the DMQT algorithm had better performance and significant advantages in label recognition time and energy consumption. To verify the performance of the DMQT anti-collision algorithm after introducing the Ack command, a comparative analysis was conducted on the total recognition time and average energy consumption of the DMQT algorithm before and after introducing the Ack command. The comparison results were shown in Figure 13.

From Figure 13 (a), before introducing the Ack command, the maximum total recognition time of the DMQT algorithm was 2.98s. After introducing the Ack command, when the probability of capture effect occurrence was 0, the maximum total recognition time of the DMQT algorithm was 3.01s. When the probability of capture effect occurrence was 0.2, 0.4, and 0.6, the maximum total recognition time of the DMQT algorithm was 3.24, 3.37, and 3.48, respectively. After introducing the Ack command in the DMQT algorithm, the total recognition time was increased,

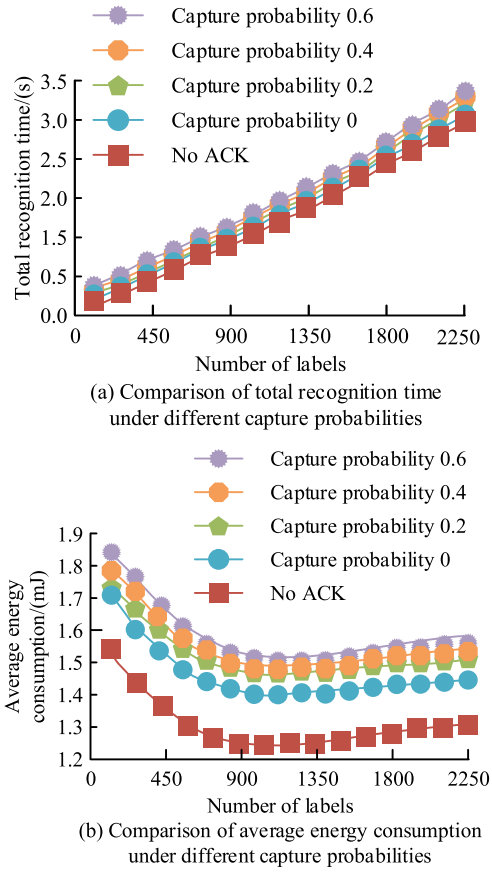

(a) Comparison of total recognition time under different capture probabilities

(b) Comparison of average energy consumption under different capture probabilities

FIGURE 13. Comparison of total recognition time and average energy consumption of DMQT algorithm before and after Ack command introduction under different probability of capture effect.

because the Ack command achieved leak free recognition. The total recognition time increased with the number of recognized tags. In Figure 13 (b), before introducing the Ack command, the maximum average energy consumption of the DMQT algorithm was 1.55mJ and the minimum value was 1.25mJ. After introducing the Ack command, when the probability of capture effect occurrence was 0, the maximum average energy consumption of the DMQT algorithm was 1.71mJ, and the minimum value was 1.39mJ. When the probability of capture effect occurrence was 0.2, 0.4, and 0.6 respectively, the maximum total recognition time of the DMQT algorithm was 1.75mJ, 1.81mJ, and 1.88mJ, while the minimum value was 1.43mJ, 1.45mJ, and 1.47mJ, respectively. After introducing the Ack command in the DMQT algorithm, the average energy consumption of the algorithm also increased, because the Ack command achieved leak free recognition, improving the recognition reliability of the DMQT algorithm.

V. CONCLUSION

To reduce the power consumption of sensing tags, a passive wireless low-power hydrogen concentration sensing system and a passive wireless magnetic field intensity sensing system are designed. In addition, to solve the low efficiency of multiple sensing tags in wireless power supply sensing systems, an efficient anti-collision algorithm based on DMQT is designed. According to the research results, in the cold start indoor environment, the energy collection rate of the sensing tag designed in the research was 0.081mJ/s, and the energy collection efficiency was 25.7%. The energy collection rates of self powered energy collection wireless sensor sensing tags and miniaturized RFID tag sensor sensing tags were 0.074mJ/s and 0.020mJ/s, respectively, with energy collection efficiency of 18.5% and 8.3%. The sensing tags designed in the research had better performance. In single/dual sensor mode, the maximum values of sensing error were 2.1% and 5.2%, respectively. In addition, under different sensor modes, the error in sensing the static magnetic field was less than 5.5%. From this, the resonant magnetic field intensity sensing tag and system had good performance. Before introducing the Ack command, the maximum total recognition time of the DMQT algorithm was 2.98s. After introducing the Ack command, when the probability of capture effect occurrence was 0, 0.2, 0.4, and 0.6, the maximum total recognition time of the DMQT algorithm was 3.01s, 3.24s, 3.37s, and 3.48s, respectively. Introducing the Ack command in the DMQT algorithm can achieve leak free recognition. However, there are also certain limitations to research. The first issue is that passive wireless sensing tags are difficult to collect weak energy. Future research can delve deeper into rectifier circuits. The second is that the DMQT anti-collision algorithm has higher requirements for the clock frequency of tags. Future research can extend the practicality of this algorithm. The third is that the reduction in label power consumption mainly focuses on system design. Future research can also start with the chip design of tags.

REFERENCES

[1] R. Priyadarshi and B. Gupta, "Area coverage optimization in three-dimensional wireless sensor network," *Wireless Pers. Commun.*, vol. 117, no. 2, pp. 843–865, Mar. 2021, doi: 10.1007/s11277-020-07899-7.

[2] D. Yang and J. Huangfu, "Improving activity recognition for multiple-node wireless sensor network system based on compressed sensing," *Int. J. Sensor Netw.*, vol. 34, no. 3, pp. 162–171, Jan. 2020, doi: 10.1504/ijsnet.2020.111235.

[3] S. S. Mohar, S. Goyal, and R. Kaur, "Optimized sensor nodes deployment in wireless sensor network using bat algorithm," *Wireless Pers. Commun.*, vol. 116, no. 4, pp. 2835–2853, Sep. 2020, doi: 10.1007/s11277-020-07823-z.

[4] C. Wang, X. Shao, Y. Meng, and J. Gao, "A physical layer network coding based tag anti-collision algorithm for RFID system," *Comput., Mater. Continua*, vol. 66, no. 1, pp. 931–945, Jan. 2020, doi: 10.32604/cmc.2020.012267.

[5] D. Xu and H. Zhu, "Sum-rate maximization of wireless powered primary users for cooperative CRNs: NOMA or TDMA at cognitive users?" *IEEE Trans. Commun.*, vol. 69, no. 7, pp. 4862–4876, Jul. 2021, doi: 10.1109/TCOMM.2021.3073952.

[6] T. T. K. Tuoi, N. Van Toan, and T. Ono, "Heat storage thermoelectric generator as an electrical power source for wireless IoT sensing systems," *Int. J. Energy Res.*, vol. 45, no. 10, pp. 15557–15568, Apr. 2021, doi: 10.1002/er.6774.

[7] Z. Luo, M. Pathmanathan, W. Han, S. Nie, and P. W. Lehn, "Analysis and design for constant current/constant voltage multi-coil wireless power transfer system with high EMF reduction," *IET Power Electron.*, vol. 15, no. 12, pp. 1144–1157, Sep. 2022, doi: 10.1049/pel2.12298.

[8] M. M. Samsami and N. Yasrebi, "Novel RFID anti-collision algorithm based on the Monte–Carlo query tree search," *Wireless Netw.*, vol. 27, no. 1, pp. 621–634, Jan. 2021, doi: 10.1007/s11276-020-02466-1.

[9] C. Jing, Z. Luo, Y. Chen, and X. Xiong, "Blind anti-collision methods for RFID system: A comparative analysis," *Infocommunications J.*, vol. 12, no. 3, pp. 8–16, Jan. 2020, doi: 10.36244/icj.2020.3.2.

[10] Y. Ai, T. Bai, Y. Xu, and W. Zhang, "Anti-collision algorithm based on slotted random regressive-style binary search tree in RFID technology," *IET Commun.*, vol. 16, no. 10, pp. 1200–1208, Jun. 2022, doi: 10.1049/cmu2.12247.

[11] X. Xuan and K. Li, "Efficient anti-collision algorithm for RFID EPC Generation-2 protocol based on continuous detection," *Int. J. Wireless Inf. Netw.*, vol. 27, no. 1, pp. 133–143, Mar. 2020, doi: 10.1007/s10776-019-00465-4.

[12] Z. Luo, C. Jing, Y. Chen, and X. Xiong, "A new underdetermined NMF based anti-collision algorithm for RFID systems," *ISA Trans.*, vol. 123, pp. 472–481, Apr. 2022, doi: 10.1016/j.isatra.2021.06.001.

[13] J. Su, Z. Sheng, A. X. Liu, Y. Han, and Y. Chen, "A group-based binary splitting algorithm for UHF RFID anti-collision systems," *IEEE Trans. Commun.*, vol. 68, no. 2, pp. 998–1012, Feb. 2020, doi: 10.1109/TCOMM.2019.2952126.

[14] S. Samizade, C. Shen, C. Si, and X. Guan, "Passive browser identification with multi-scale convolutional neural networks," *Neurocomputing*, vol. 378, pp. 238–247, Feb. 2020, doi: 10.1016/j.neucom.2019.10.028.

[15] B. D. B. Chowdhury, S. Masoud, Y. J. Son, C. Kubota, and R. Tronstad, "A dynamic data driven indoor localisation framework based on ultra high frequency passive RFID system," *Int. J. Sensor Netw.*, vol. 34, no. 3, pp. 172–187, Jan. 2020, doi: 10.1504/ijsnet.2020.111236.

[16] K. Dong, Y. Chu, X. Tian, T. Fang, X. Ye, X. Wang, and F. Tang, "Wearable photoelectric fingertip force sensing system based on blood volume changes without sensory interference," *ACS Appl. Mater. Interfaces*, vol. 15, no. 29, pp. 34578–34587, Jul. 2023, doi: 10.1021/acsami.3c06469.

[17] S. D. M. Achanta and T. Karthikeyan, "A wireless IoT system towards gait detection technique using FSR sensor and wearable IoT devices," *Int. J. Intell. Unmanned Syst.*, vol. 8, no. 1, pp. 43–54, Jul. 2019, doi: 10.1108/ijius-01-2019-0005.

[18] D. Wang, J. Hu, J. Wang, Y. Ding, and J. Wu, "VLSI implementation of area and power efficient digital control circuit for HF RFID tag chip," *Chin. J. Electron.*, vol. 29, no. 1, pp. 82–88, Jan. 2020, doi: 10.1049/cje.2019.10.003.

[19] N. Suess, T. Hartmann, and N. Weisz, "Differential attention-dependent adjustment of frequency, power and phase in primary sensory and frontoparietal areas," *Cortex*, vol. 137, pp. 179–193, Apr. 2021, doi: 10.1016/j.cortex.2021.01.008.

[20] R. L. Germano, M. M. Oliveira, and E. S. L. Gastal, "Real-time frequency adjustment of images and videos," *Comput. Graph. Forum*, vol. 40, no. 2, pp. 23–37, May 2021, doi: 10.1111/cgf.142612.
[21] X. Yuan, N. Wang, W. Wang, L. Zhang, and Y. Zhu, "Nozzle resonance mechanism and cooperative optimization of self-excited oscillating pulse cavitation jet," *Trans. Can. Soc. Mech. Eng.*, vol. 47, no. 1, pp. 74–88, Mar. 2023.
[22] S. Babu and L. A. Kumar, "Voltage controller with energy management unit for microgrid with hybrid sources," *Energy Explor. Exploitation*, vol. 39, no. 6, pp. 2126–2149, Jun. 2021, doi: 10.1177/01445987211015392.
[23] A. S. Maihulla, I. Yusuf, and S. I. Bala, "Reliability and performance analysis of a series-parallel system using Gumbel–Hougaard family copula," *J. Comput. Cognit. Eng.*, vol. 1, pp. 74–82, Oct. 2021, doi: 10.47852/bonviewjcce2022010101.
[24] A. A. Gouda and A. S. Amin, "Design of a novel optical sensor for determination of trace amounts of tin in food and in environmental samples," *Int. J. Environ. Anal. Chem.*, vol. 102, no. 18, pp. 7313–7328, Dec. 2022, doi: 10.1080/03067319.2020.1830988.
[25] M. Prabha, S. S. Darly, and B. J. Rabi, "A novel approach of hierarchical compressive sensing in wireless sensor network using block tri-diagonal matrix clustering," *Comput. Commun.*, vol. 168, pp. 54–64, Feb. 2021, doi: 10.1016/j.comcom.2020.12.017.
[26] Z. A. Khan, T. Hussain, U. Zabit, M. Usman, and E. Ayguade, "PH-RLS: A parallel hybrid recursive least square algorithm for self-mixing interferometric laser sensor," *IET Optoelectron.*, vol. 15, no. 5, pp. 239–247, Mar. 2021, doi: 10.1049/ote2.12021.
[27] Q. D. To and G. Bonnet, "Fourier transform approach to homogenization of frequency-dependent heat transfer in porous media," *Int. J. Numer. Methods Heat Fluid Flow*, vol. 33, no. 6, pp. 2023–2048, May 2023, doi: 10.1108/hff-03-2022-0198.
[28] Z. Wang, F. Gao, Y. Zhao, Y. Yin, and L. Wang, "Improved A* algorithm and model predictive control- based path planning and tracking framework for hexapod robots," *Ind. Robot: Int. J. Robot. Res. Appl.*, vol. 50, no. 1, pp. 135–144, Jan. 2023, doi: 10.1108/ir-01-2022-0028.
[29] B. C. Ahn, J. W. So, C. B. Synn, T. H. Kim, J. H. Kim, Y. Byeon, Y. S. Kim, S. G. Heo, S. D. Yang, M. R. Yun, and S. Lim, "Clinical decision support algorithm based on machine learning to assess the clinical response to anti-programmed death-1 therapy in patients with non-small-cell lung cancer," *Eur. J. Cancer*, vol. 153, pp. 179–189, Aug. 2021, doi: 10.1016/j.ejca.2021.05.019.
[30] X. Wang, Z. Xia, X. Zhou, J. Wei, X. Gu, and H. Yan, "Collision-free path planning for arc welding robot based on ida-de algorithm," *Int. J. Robot. Autom.*, vol. 37, no. 6, pp. 476–485, May 2022, doi: 10.2316/j.2022.206-0611.
[31] P. Zhang, H. Yue, Z. Shi, J. Lin, and Z. Chen, "A fuzzy PID algorithm-based attitude control method of suspension-type small rail vehicles," *J. Vibrat. Eng. Technol.*, vol. 10, no. 1, pp. 111–130, Jan. 2022.
[32] R. A. Fahmy and R. I. Gomaa, "Dynamic fault tree analysis of auxiliary feedwater system in a pressurized water reactor," *Kerntechnik*, vol. 86, no. 2, pp. 164–172, Apr. 2021, doi: 10.1515/kern-2020-0067.
[33] J. N. Yasin, S. A. S. Mohamed, M.-H. Haghbayan, J. Heikkonen, H. Tenhunen, and J. Plosila, "Low-cost ultrasonic based object detection and collision avoidance method for autonomous robots," *Int. J. Inf. Technol.*, vol. 13, no. 1, pp. 97–107, Feb. 2021, doi: 10.1007/s41870-020-00513-w.
[34] W. Zhu, Z. Pang, J. Si, and Z. Du, "Collision response and obstacle avoidance of the tethered-space net robot system with non-target objects," *Aircr. Eng. Aerosp. Technol.*, vol. 94, no. 5, pp. 715–733, Jan. 2022, doi: 10.1108/aeat-07-2021-0208.
[35] S. Pappan and P. Anandhakumar, "RMF based target position estimation and collision probability forecasting technique in freeway junctions," *Int. J. Heavy Vehicle Syst.*, vol. 27, no. 1, pp. 145–163, Jan. 2020, doi: 10.1504/ijhvs.2020.104410.
[36] W. Xie, M. Cui, M. Liu, P. Wang, and B. Qiang, "Deep hashing multi-label image retrieval with attention mechanism," *Int. J. Robot. Autom.*, vol. 37, no. 4, pp. 372–381, Jun. 2022.
[37] C. Hua, Z. Sun, and Z. Chen, "Stabilization for time-delay nonlinear systems with unknown time-varying control coefficients," *J. Franklin Inst.*, vol. 359, no. 16, pp. 8895–8909, Nov. 2022.
[38] Z. L. Hailemariam, Y.-C. Lai, R. Jayadi, Y.-H. Chen, and S.-C. Huang, "A knowledge-based query tree with shortcutting and couple-resolution for RFID tag identification," *Comput. Commun.*, vol. 160, pp. 779–789, Jul. 2020, doi: 10.1016/j.comcom.2020.06.025.
[39] T. Gagie, M. He, G. Navarro, and C. Ochoa, "Tree path majority data structures," *Theor. Comput. Sci.*, vol. 833, pp. 107–119, Sep. 2020, doi: 10.1016/j.tcs.2020.05.039.
[40] R. Srinivasan and U. H. Hyder Ali, "Energy harvesting wireless sensor for achieving self-powered structural health monitoring system," *Circuit World*, vol. 46, no. 4, pp. 307–315, Mar. 2020, doi: 10.1108/cw-05-2019-0045.
[41] P. Wang, L. Dong, H. Wang, G. Li, Y. Di, X. Xie, and D. Huang, "Investigation the influence of miniaturized RFID tag sensor on coupling effect," *Sensor Rev.*, vol. 41, no. 4, pp. 425–435, Sep. 2021, doi: 10.1108/sr-04-2021-0138.

DANENG PI was born in Xianning, Hubei, in 1966. He received the bachelor's degree in industrial electrical automation and the master's degree in power electronics and power transmission, in 1996 and 2001, respectively. From 1986 to 2005, he was a Lecturer with Hubei University of Technology. Since 2005, he has been an Associate Professor with Hubei Normal University. He has published more than 40 papers, participated in eight research projects, authored seven textbooks, and obtained five patents.